CHAPTER 3

Rotation and Single-Particle Motion

3.1 Introduction

The experimental level schemes of nuclei show an enormous complexity. On the way to understanding at least the basic features of their structure, we have introduced in the first part of this book two rather contrasting models: On the one hand the liquid drop model describes collective phenomena, such as vibrations and rotations, where many nucleons are involved. On the other hand the shell model treats the individual nucleons as independent particles and provides an understanding of single-particle excitations. However, these two models are only limiting cases that are never realized exactly in nature. We always have some deviations and we usually find all kinds of transitions between these extreme models.

For a deeper understanding of the underlying structures, we have to solve, in principle, the nuclear many-body problem and investigate in which limits solutions are provided corresponding to the above simple phenomenological pictures, and in which cases new models must be introduced to obtain a simple description. In the following chapters of this book, we will treat such microscopic methods in much detail, and will reproduce many of the results of the phenomenological models. Although such theories are extremely useful for an understanding of principal questions, they usually involve a terrible amount of numerical effort and are not very useful for a fast and qualitative interpretation of experimental data.

Therefore, it seems to be worthwhile going further on the phenomenological path in this chapter and trying to describe more complicated spectra by a combination of the collective model and the single-particle model. In the last chapter, we saw that such a combination is very useful in describing bulk properities such as nuclear binding energies and deformations. In that case, we had to deal with fluctuations of the level density, and we did not have to take into account the individual degrees of freedom in detail. Now we want to describe individual spectra. For this we have to again try a combination of the single-particle and collective models. We can, for instance, couple one or a few particles to a collective rotor or vibrator. This so-called "*unified model*" was introduced by Bohr and Mottelson [Bo 52, BM 53], and has been described in great detail in many textbooks (see, for instance, [Da 68, EG 70, Ro 70, SF 74, or BM 75]). In the case of collective vibrations, we will deduce the corresponding Hamiltonian and discuss the model of a particle coupled to a vibrator in Chapter 9. In the case of rotations, such a derivation from first principles has been missing till now. Methods have been developed to describe rotations microscopically (see Chap. 11), but they turn out to be extremely complicated. Only in the limit of strong deformations is it possible to deduce a simple rotational model, the cranking model.

In the last few years considerable experimental effort has been made to investigate rotations, and a great variety of new phenomena has been observed. Since these phenomena can be understood to a large extent by the interplay between single-particle motion and collective rotational motion, we think it is necessary to introduce in this chapter two theoretical but phenomenological models which deal with these effects.

In Section 3.2 we give a general survey of the features one expects in rotating nuclei. In Section 3.3 we discuss the rotational part of the unified model, the so-called particle-plus-rotor model (PRM), and in Section 3.4 we present the microscopic cranking model.

We want to emphasize, however, that we do not give a complete description of nuclear rotation in this chapter. The residual interactions in the form of pairing correlations play an important role in this context. They will be treated in Chapter 7.

3.2 General Survey

3.2.1 Experimental Observation of High Spin States

New experimental techniques, namely, heavy ion fusion reactions [MG 63, SLD 65], Coulomb excitation with heavy projectiles [HZ 53, AW 66, 74, WCL 76], and pion capture reactions [EAD 75] have made it possible to excite nuclear states with angular momenta large enough to generate major modifications in the nuclear structure (for a review, see [JS 73, St 76, LR 78]).

The most important such reactions are of the (HI, xn) type, where one bombards the target with heavy ions (α, Ne, Ar, etc.) carrying a large amount of orbital angular momentum. After fusion, the combined system evaporates some neutrons and ends up in highly excited states with very large spin (depending on the projectile and the incoming energy up to $\sim 100\ \hbar$). This highly excited final nucleus then de-excites in a cascade of γ-radiation. The fastest transitions are *statistical E1-transitions*. They carry away much energy, but only a few units of angular momentum. In a plot of the energy versus the angular momentum (Fig. 3.1), these statistical cascades correspond to nearly vertical lines. They end up at the so-called *yrast line*,* the line which connects the levels of lowest energy to each angular momentum (or the levels with highest angular momentum at a given energy). The rest of the cascade has to follow this line. For deformed nuclei these are *collective E2-transitions* ($\Delta I = 2$), which finally go over into the well-known ground state rotational band (see Sec. 1.5).

Until now, only the last part of these cascades could be resolved into discrete lines (see Fig. 3.5). The highest angular momenta observed in this way lie between 30 and 40 $\hbar$. The rest of the cascade is measured as a γ-continuum, and one can draw only indirect conclusions from these data [GG 67, BSC 75, SBC 76, Di 76, HLM 78, ABH 78, WF 78b]. There are, however, indications that collective transitions along lines parallel to the yrast line (see Fig. 3.1) play an important role, and that there is a

* The Swedish word *yrast* means "fastest rotating" [Gr 67]. One also uses the name *yrare* for the level with the second lowest energy at each I-value.

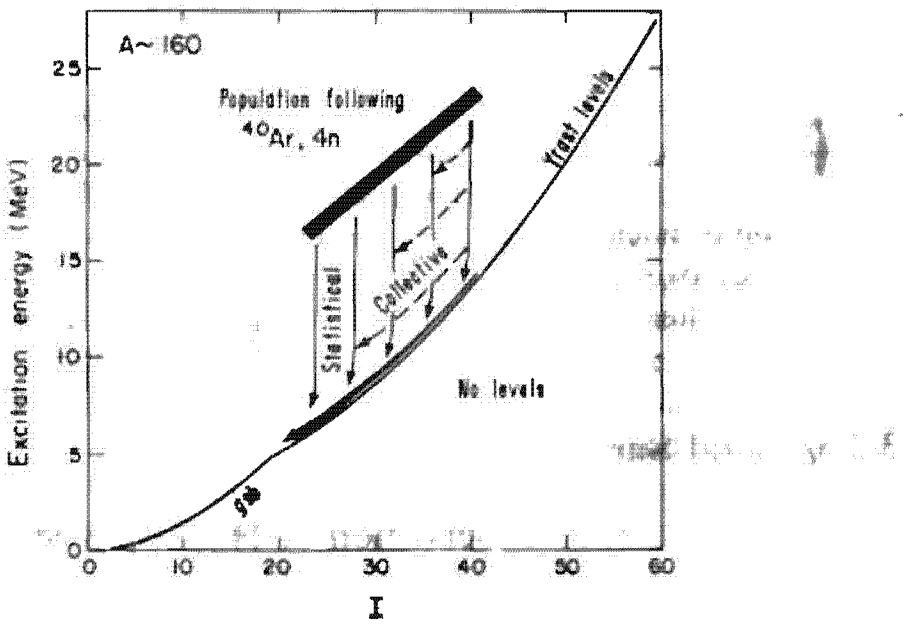

Figure 3.1. Excitation energy as a function of angular momentum I for the reaction (^{40}Ar, $4n$). After the evaporation of four neutrons, the nucleus decays by a γ-cascade of statistical $E1$- and collective $E2$-transitions down to the yrast line, and then to the ground state by a series of $E2$-transitions along this line. The yrast band shows an increasing intensity, because it collects all the statistical transitions ("side feeding"). (From [SBD 77].)

competition between collective and statistical effects in the region of a few MeV above the yrast line [SBD 77].

3.2.2 The Structure of the Yrast Line

In Section 1.7 we saw that a *classical liquid drop* [CPS 74] rotates at low angular frequencies around the symmetry axis of its oblate shape (Hiskes regime, Fig. 3.2a). Only for very high angular velocities does it undergo a phase transition to the Beringer–Knox regime, where it has a triaxial, but nearly prolate, shape and the rotational axis is perpendicular to the approximate symmetry axis (Fig 3.2b). For still higher frequencies it finally fissions (Fig. 3.2c).

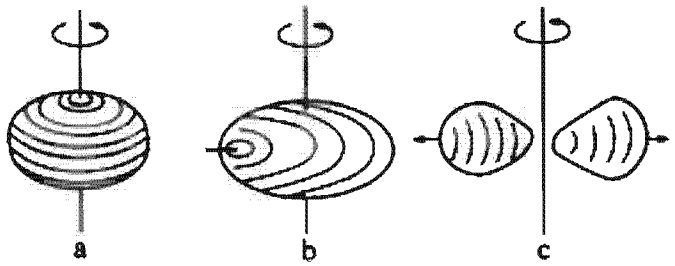

Figure 3.2. The behavior of a classical liquid drop for increasing angular velocity.

The *real nucleus*, however, is a quantum mechanical system. It shows shell effects (see Chap. 2.9), which cause stable deformations already in the ground state for some regions of the periodic table. The yrast line corresponds to the lowest energy for each angular momentum; all the excitation energy of several tens of MeV with respect to the ground state is rotational energy and used to generate angular momentum. Consequently, the level density along this line is low, much lower than the level density of the $I=0$ states at the corresponding energy. It resembles that of the ground state, though we will see that there are characteristic deviations from it. Since the nucleus is cold in the yrast region, we can expect a high degree of order. Shell effects play an important role.

The prolate deformations caused by the shell effects are of the same order of magnitude as the oblate deformations of a classical drop at high angular velocities (see Sec. 1.7). We therefore expect a delicate interplay between macroscopic centrifugal effects and microscopic shell structure when we study the nuclear shapes as a function of the angular momentum.

Let us first study the case of well-deformed heavy nuclei (for instance, in the rare earth region). In the ground state they show a prolate axial symmetric quadrupole deformation caused by shell effects. The levels in the corresponding deformed potential are occupied pairwise by nucleons with the opposite single-particle angular momentum ($\pm\Omega$). We will see in Chapter 6 that the two nucleons in such a pair do not move independently, as was assumed in the last chapter, but are coupled by a pairing force to the so-called Cooper pairs with spin zero; that is, these deformed nuclei

show a *superfluid behavior* and their ground state energy is lowered by a few MeV.

With increasing angular momentum, we can distinguish several regimes where the yrast states show quite a different structure [BM 74]:

(a) For low angular momenta $I = 0, 2, 4, \ldots$, the yrast line follows the *ground state rotational band*, as discussed in Section 1.5. The rotation is collective, that is, it has to be perpendicular to the symmetry axis (see Fig. 3.3a, where we have indicated the coupled pairs of nucleons oriented along the symmetry axis).

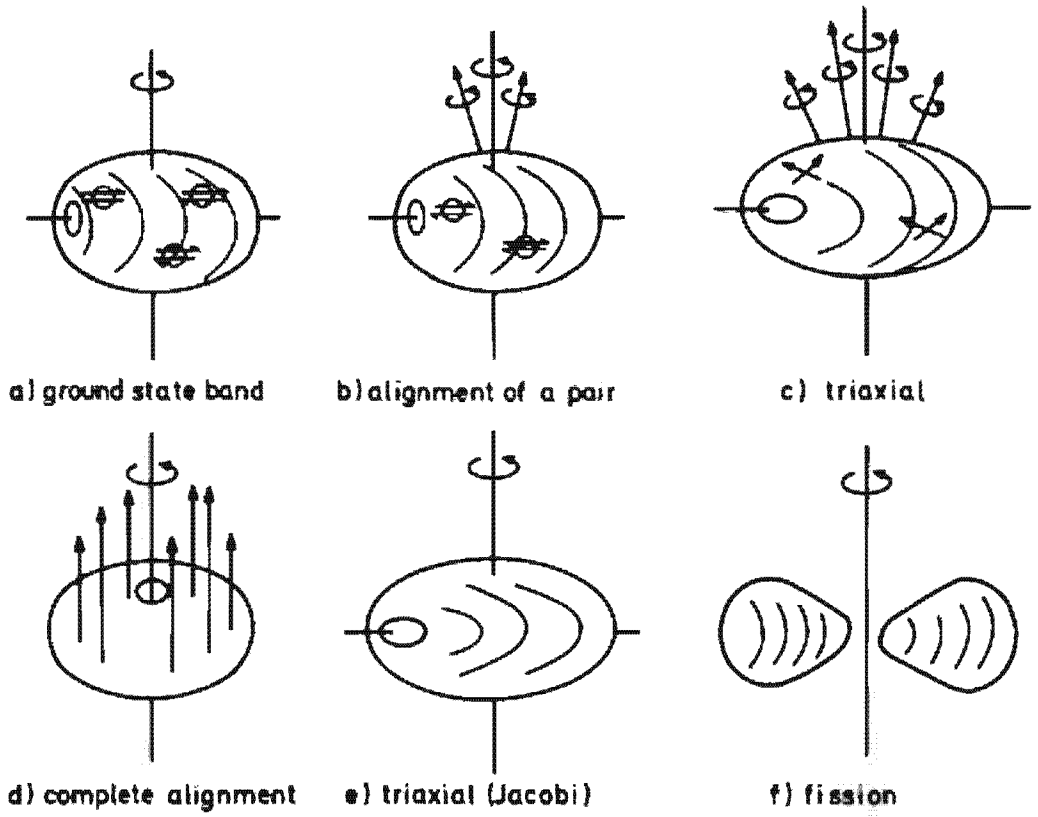

Figure 3.3. Possible structures along the yrast line of a deformed nucleus.

The nucleus feels a slowly rotating deformed potential (for a more detailed discussion, see Sec. 3.4). The Coriolis forces act on both spins of a pair with opposite angular momenta $\pm\Omega$ in opposite directions and try to align them parallel to the rotational axis, that is, they try to break the Cooper pairs [*Coriolis anti-pairing (CAP) effect*]. However, for low angular momenta the Coriolis forces are weak and unable to break pairs: The nucleus rotates more or less with the same structure as the ground state.

We have to emphasize, however, that in a microscopic picture the total angular momentum has to be generated by the angular momenta of single nucleons. In a collective rotation this is achieved by aligning all the particles a little bit in the direction of the rotational axis. For each pair this effect is very small; the spins of the pairs are still oriented nearly anti-parallel along the symmetry axis of the potential. By summing up all the small contributions we obtain the total angular momentum $I = 2, 4, \ldots, .$

(b) Going to higher and higher angular momenta, the Coriolis force, increases more and more and at a certain angular momentum it will be able to break pairs. Therefore, at some critical angular momentum I_c we expect that all pairs are broken. The pairing correlations break down completely and a *phase transition* from the superfluid phase to the normal phase is observed. This effect was predicted by Mottelson and Valatin in 1960 [MV 60]. More detailed investigations, however, have shown that the Coriolis force is proportional to the size of the single-particle angular momentum j of the nucleon under consideration. We have seen in Section 2.8 that the nucleons in the vicinity of the Fermi surface belong to subshells with rather different j-values, and we expect those nucleons with large j-values to align first along the rotational axis. These are usually the levels with high spin and opposite parity, shifted downwards by the spin orbit term, as for instance the $i_{13/2}$ shell for neutrons in the rare earth region (Stephens–Simon effect [SS 72a]).

In the second regime of the yrast line (Fig. 3.3b), we therefore expect *alignment processes* of one or the other broken pairs, whereas the rest of the nucleus stays more or less unchanged. The yrast band can then no longer be identified with the ground state band, but rather with a band of two aligning particles sitting on the rotating core. Two $i_{13/2}$ particles can contribute 12 units of angular momentum to the rotation. Such an alignment is therefore connected with a rapid increase of the angular momentum I as a function of the collective angular velocity and leads to a series of anomalies in the spectra [JRS 71, JRH 72], for example, the "back-bending phenomenon" (see below).

(c) Each alignment process is connected with a certain change in the collective properties by its influence on the mean field: Broken pairs no longer contribute to the pairing correlations; because of the blocking effect (see Sec. 6.3.4.) these correlations will disappear completely after a few alignments. Particles aligned to the rotational axis have an oblate density distribution, with the rotational axis as the symmetry axis. We therefore get triaxial admixtures to the prolate density distribution of the core.

In a third regime (Fig. 3.3c) which should correspond roughly to angular momenta $30 \lesssim I \lesssim 50$, we expect the Coriolis and centrifugal forces to produce effects comparable in strength to the shell structure effects, namely, changes in the shapes to *triaxial deformations*. Such a system without a symmetry axis shows more collective states than the axial symmetric rotor (see Sec. 1.5.3): We expect a sequence of rotational states parallel to the yrast line corresponding to a *wobbling motion*.

(d) If an essential part of the nucleons are aligned parallel to the rotational axis, we finally expect an *axially symmetric oblate shape*.

The nuclear wave function is symmetric with respect to rotations around this axis. The rotation is no longer collective. Instead, the total angular momentum is made up by reoccupation of distinct particles in the deformed well.

This kind of motion is called *"single-particle" rotation*. The energy of the states along the yrast line in this region is determined by the single-particle energies in the rotating oblate well. The energy differences between adjacent states vary statistically. Only on the average do they follow an $I \cdot (I+1)$ law with the moment of inertia of a rigid rotor (see Sec. 3.4.6.). The transition from one state to the next corresponds to a reoccupation, and the matrix elements should adopt single-particle values, that is, the transition probability should be drastically reduced.

Because of the statistical nature of the levels in that region of the yrast line, one also expects long lived *high spin isomeric states*, so-called *yrast traps* [BM 74] which could eventually produce a delayed decay such that we could observe the whole yrast cascade of discrete lines without the background of all statistical transitions.

(e) For very large angular momenta we finally expect only the macroscopic properties to be essential, that is, the nucleus should again undergo a transition from oblate to triaxial and prolate shapes before it fissions (Fig. 3.3e, f).

So far, only discrete levels in the regimes (a) and (b) have been observed; the rest of these considerations is to a large extent speculation. We will see in Sec. 3.4.5 the kind of models one has used to obtain theoretical predictions. In fact, in the calculations one has found all the different regimes discussed above.

It seems to be possible, however, that many nuclei do not pass through all these stages. In particular, weakly deformed or spherical nuclei adopt from the beginning the regime (d), namely, a rotation of an oblate shape around the symmetry axis before going triaxial and fissioning. On the other hand, in many well-deformed nuclei the change in deformation produced by the alignment processes is not strong enough to compensate the shell effect of a prolate deformation. They only become triaxial (Fig. 3.3c, d), not oblate, before fissioning. Experimentally, one has observed longliving high spin isomers (yrast traps) only for weakly deformed nuclei (see Sec. 3.4.6). This seems to be in agreement with theoretical calculations.

Besides the yrast band, one has observed many other rotational bands in the low and *medium spin region*. They are based on more complex configurations, such as quasi-particle excitations or vibrational states.

Depending on the size of the j shell orbitals, which are involved in such configurations, one can imagine a large variety of alignment processes. For example, in an odd mass nucleus the alignment of the odd neutron in the $i_{13/2}$ shell, which leads to so-called *decoupled bands*. Another example is the rotational band in an odd-odd nucleus, where only the neutron in the $i_{13/2}$

shell aligns, whereas the proton stays oriented along the symmetry axis. Such a band has a *semidecoupled* structure [NVR 75].

The particle-plus-rotor model discussed in Section 3.3 provides a phenomenological method to describe such processes. In that section we will come back to some examples of this type in more detail.

3.2.3 Phenomenological Classification of the Yrast Band

Over the years some phenomenological models have been introduced to characterize the properties of rotational bands. In the low spin region (Fig. 3.3a), the spectra often follow exactly the $I\cdot(I+1)$ law, but for higher I-values there occur deviations to a greater or lesser extent*. In order to describe the deviations from the ideal rotational spectrum, one often applies the following parametrization:

$$E(I)=A\cdot I\cdot(I+1)+B\cdot(I(I+1))^2+C\cdot(I(I+1))^3+\cdots. \tag{3.1}$$

It turns out that in many cases the convergence of this expansion is rather poor and an expansion in the *angular frequency* ω is more appropriate.

In principle, ω is not a measurable quantity. We can define it, however, semiclassically as

$$\omega=\frac{dE}{dJ}, \qquad \text{with} \quad J=\sqrt{I(I+1)}\ . \tag{3.2}$$

Replacing the differential quotient by a quotient of finite differences,† we obtain a definition of an "experimental" value for the *angular velocity*‡

$$\omega_{\exp}\simeq\frac{\Delta E}{\Delta\sqrt{I(I+1)}}\bigg|_{I,\,I-2}\simeq\frac{E(I)-E(I-2)}{\sqrt{I(I+1)}-\sqrt{(I-2)(I-1)}}\ . \tag{3.3}$$

The *moment of inertia* is defined by

$$\mathcal{I}=\frac{J}{\omega}=\frac{1}{2}\left(\frac{dE}{dJ^2}\right)^{-1}\simeq\frac{2I-1}{\Delta E_{I,\,I-2}}\ . \tag{3.4}$$

With these definitions, we can calculate values of ω and $\mathcal{I}$ for each level of the yrast band.

Harris [Ha 65a] proposed the following parametrization of the spectrum:

$$E(I)=\alpha\omega^2+\beta\omega^4+\gamma\omega^6+\cdots. \tag{3.5}$$

Odd powers in ω do not occur, since E cannot change by reversing the angular velocity. For ω as a function of I we can either choose the experimental value (3.3) or avoid the ambiguity of its definition by using a similar expansion of J. From

$$\frac{dE}{d\omega}=\frac{dE}{dJ}\frac{dJ}{d\omega}=\omega\frac{dJ}{d\omega} \tag{3.6}$$

we obtain

$$J(I)=\sqrt{I(I+1)}\ =2\alpha\omega+\frac{4}{3}\beta\omega^3+\frac{6}{5}\gamma\omega^5+\cdots.$$

* For a compilation of such data, see [SHJ 73, SSM 75].

† This replacement is not unique, however, and some groups use different prescriptions (see [JS 73, So 73, LR 78]).

‡ Within this chapter we always use the units $\hbar=1$.

Of course, this expansion is valid only as long as J is not a multivalued function of ω, that is, it is of no use in the backbending region (see Sec. 3.2.4.).

Another model which is widely used for the classification of rotational and even transitional nuclei is the *variable moment of inertia* (VMI) model [MSB 69, SDG 76]. The moment of inertia $\mathcal{I}$ is considered as a variable on which the intrinsic energy V depends:

$$E(I, \mathcal{I}) = \frac{1}{2\mathcal{I}} I(I+1) + V(\mathcal{I}). \tag{3.7}$$

According to the variation principle (discussed in Sec. 5.2), the total energy E has to be minimized for a fixed value of I with respect to $\mathcal{I}$. This determines the functional dependence $\mathcal{I}(I)$. Assuming we know $V(\mathcal{I})$, $\mathcal{I}(I)$ is implicity given by

$$\left.\frac{dE}{d\mathcal{I}}\right|_I = -\frac{1}{\mathcal{I}} \frac{I(I+1)}{2\mathcal{I}} + \frac{dV}{d\mathcal{I}} = 0.$$

Usually one expands on $V = \frac{1}{2} C(\mathcal{I} - \mathcal{I}_0)^2$, where $\mathcal{I}_0$ is the value of $\mathcal{I}$ at $I = 0$. The coefficients C and $\mathcal{I}_0$ are adjusted to the experimental spectrum $E(I)$. With the identification $J = \omega \cdot \mathcal{I}$ this corresponds to the Harris model to order ω^4, but the ansatz (3.7) is certainly more general [DB 73, SDG 76].

3.2.4 The Backbending Phenomenon

In the region between 10 and 20 units of angular momentum, an anomaly is observed in the yrast band of many nuclei. It can be most easily demonstrated if one plots the moment of inertia $\mathcal{I}$ as a function of ω^2. In lowest order in the VMI model ($\mathcal{I} = \mathcal{I}_0 + b\omega^2 + \cdots$) this should give a straight line. The deviation from a constant is then a measure of the validity of the $I \cdot (I+1)$ law. Figure 3.4 gives two examples for such curves, measured by the Jülich group [LR 78].

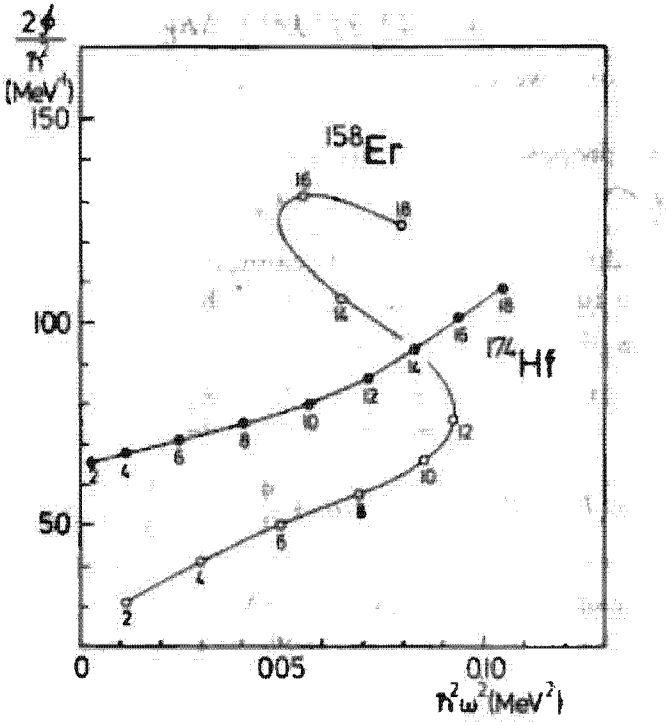

Figure 3.4. Moment of inertia $\mathcal{I}$ as a function of the rotational frequency squared for ^{158}Er and ^{174}Hf

For low spin values one indeed finds straight lines. In the nucleus ^{174}Hf the deviations are, in fact, smooth. In ^{158}Er, however, a very steep increase occurs for certain I values, the curve even bending backwards, ("back-bending" phenomenon [JRH 72]). This means experimentally that the transition energy $\Delta E_{I,I-2}$, which should increase linearly with I for the constant rotor as

$$\Delta E_{I,I-2} = \frac{1}{2\mathfrak{I}}(4I-2), \tag{3.8}$$

does not increase, but decreases for certain I values. Figure 3.5 shows the experimental data that correspond to Figure 3.4.

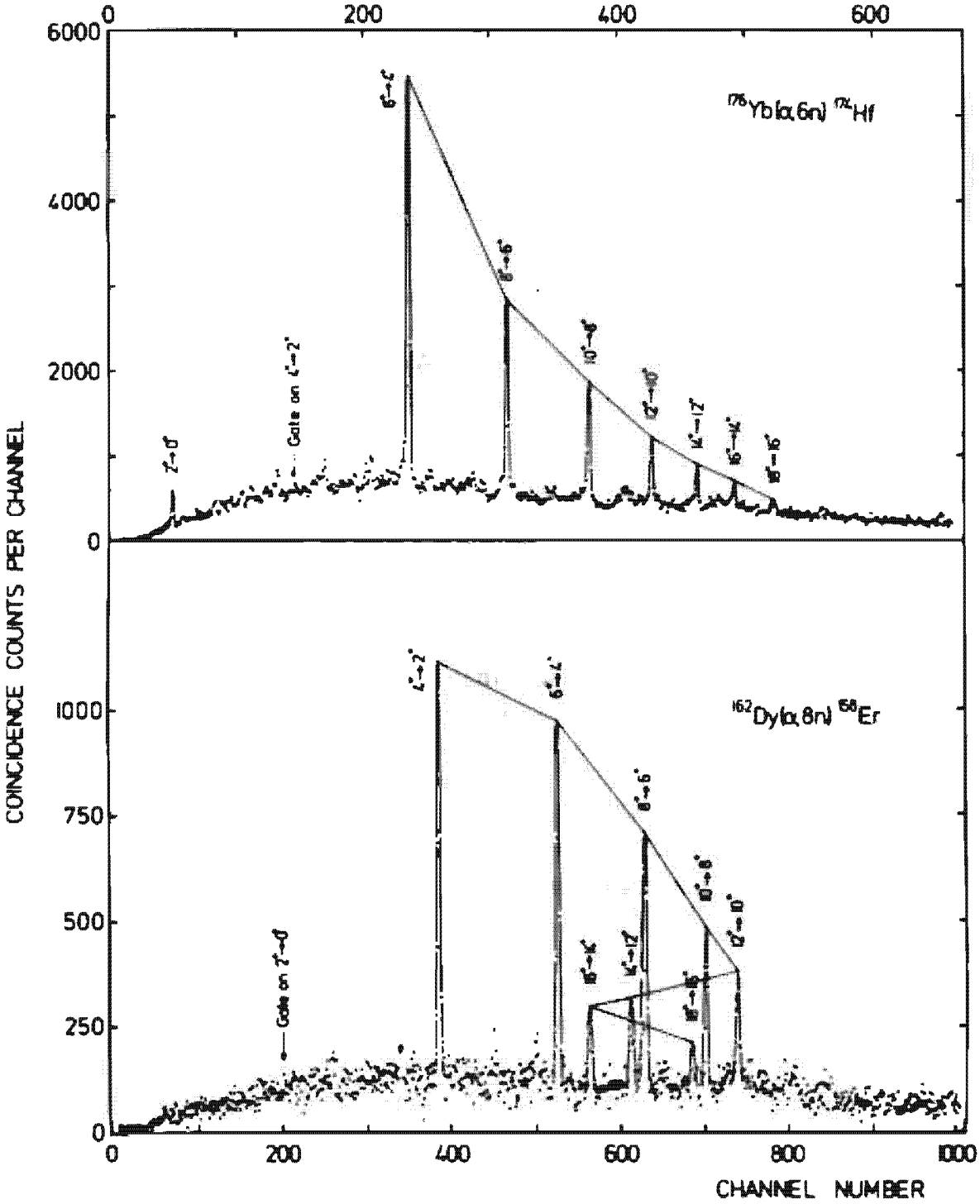

Figure 3.5. The reactions ^{176}Yb $(\alpha, 6n)$ ^{174}Hf and ^{162}Dy $(\alpha, 8n)$ ^{158}Er. The last reaction shows the anomaly called backbending in the I region $10^+ - 14^+$. This is

Such a phenomenon can easily be reproduced as an effect due to the crossing of two bands (in some cases one has even observed the second band experimentally, see Fig. 7.6 and [KSM 78]). To see this, let us assume that the two bands have different moments of inertia (Fig. 3.6) corresponding to two parabolas in an E versus I plot. If $\mathcal{I}_2 > \mathcal{I}_1$ the bands cross in a certain region of I. Because of the residual interaction, such a crossing does not take place (the no-crossing rule; see Sec. 2.8.4), and we can get a region in which the second derivative is negative:

$$0 > \frac{d^2E}{dI^2} = \frac{d\omega}{dI}. \tag{3.9}$$

This means we have an increasing I with decreasing ω, while at the same time the properties of the bands are exchanged. In fact, it is easy to fit such backbending curves by a band mixing calculation with few parameters, one of which is the interaction V between the bands. For small values of V, one obtains a sudden transition which produces backbending, whereas for large values of V the transition region is very broad and no backbending occurs [MR 72, GG 74b].

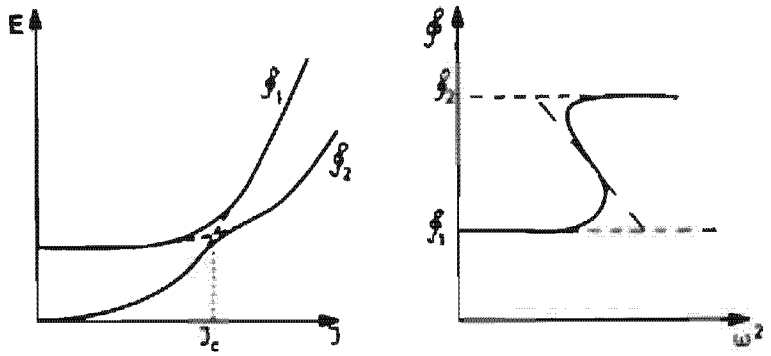

Figure 3.6. Schematic picture of two intersecting bands with different moments of inerita $\mathcal{I}_1$ and $\mathcal{I}_2$, and the corresponding backbending plot. (From [LR 78].)

On the other hand, it is also clear that the strange backbending behavior in the plot of the moment of inertia $\mathcal{I}$ against ω^2 has its origin in the fact that we follow the yrast line in the critical region, that is, we switch over to the crossing band with a different internal structure. If we would stay in the ground state band, which is no longer the yrast band for the large I-values, we would obtain a very smooth behavior for the ω-dependence of the moment of inertia (dashed-line in Fig. 3.6). The reason that one usually follows the yrast band is that these levels are experimentally the most easily accessible.

In all of these considerations, one should, however, keep in mind that these kinds of phenomenological descriptions only give a classification of the spectra and do not say anything about their physical origin. In the case of backbending there is, for instance, the question concerning the nature of the second band. Three types of theoretical interpretations have been given:

(i) In the second band the nucleus has a different deformation, for

instance, a triaxial one. This means that backbending is caused by a sudden change of deformation [Th 73, SV 73].

(ii) The second band is not superfluid, as in the ground state band. This would interpret backbending as a phase transition from a superfluid to a normal-fluid state (Mottelson–Valatin effect [MV 60]).

(iii) The second band is a two quasi-particle band of particles which are rotationally aligned along the axis of rotation (see Sec. 3.3). Then backbending would correspond to a sudden alignment of a pair of nucleons (as proposed by Stephens and Simon [SS 72a]).

The general result of theoretical investigations, which include all these degrees of freedom (see Sec. 7.7), is that for the well deformed nuclei (the classical rotors) the reduction of the pairing correlations is only responsible for the slow change of the moment of inertia at low spin values, but that sudden effects such as backbending are due to alignment of a single high j pair of nucleons. There is also a large number of experimental indications [GSD 73, RSS 74, WBB 75, NLM 76, St 76] for this interpretation of the backbending phenomenon.

In the rare earth nuclei, the $i_{13/2}$ neutrons play an essential role. There is, however, experimental evidence for a second irregularity at spins of $\sim$ 26–30 $\hbar$ [LAD 77, BBB 79a] a so-called *second backbending*, which has been interpreted as the alignment of an $h_{11/2}$ proton pair [FP 78]. Other high j-orbitals may play similar roles in different regions of the periodic table.

3.3 The Particle-plus-Rotor Model

To describe the interplay between the motion of particles and the collective rotation, Bohr and Mottelson [BM 53] proposed to take into account only a few so-called valence particles, which move more or less independently in the deformed well of the core, and to couple them to a collective rotor which stands for the rest of the particles. The division into core and valence particles is not always unique. It is, however, reasonable to use the unpaired nucleon in an odd mass nucleus as a valence nucleon on an even–even core. One also can attribute the particle and the hole of a particle–hole excitation to the valence particles. More generally, one divides the Hamiltonian into two parts: an intrinsic part H_{intr}, which describes microscopically a valence particle or a whole subgroup of particles near the Fermi level; and a phenomenological part H_{coll} which describes the inert core:

$$H = H_{\text{intr}} + H_{\text{coll}}. \tag{3.10}$$

The *intrinsic part* has the form

$$H_{\text{intr}} = \sum_k \epsilon_k a_k^+ a_k + \frac{1}{4} \sum_{klmn} \bar{v}_{klmn} a_k^+ a_l^+ a_n a_m, \tag{3.11}$$